Communication

Hierarchical Assembly of SnO Nanorod Arrays on -FeO Nanotubes: A Case of Interfacial Lattice Compatibility

Dong-Feng Zhang, Ling-Dong Sun, Chun-Jiang Jia, Zheng-Guang Yan, Li-Ping You, and Chun-Hua Yan

J. Am. Chem. Soc., **2005**, 127 (39), 13492-13493• DOI: 10.1021/ja054771k • Publication Date (Web): 09 September 2005

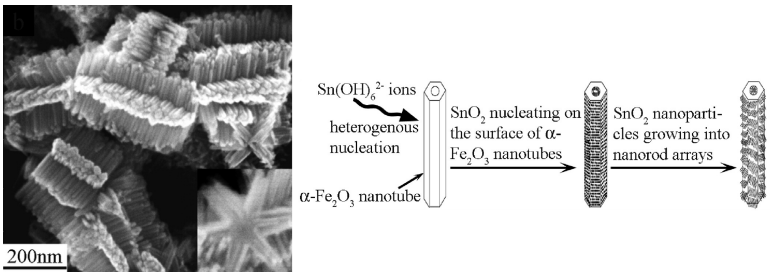

More About This Article

Additional resources and features associated with this article are available within the HTML version:

- Supporting Information
- Links to the 24 articles that cite this article, as of the time of this article download
- Access to high resolution figures
- Links to articles and content related to this article
- Copyright permission to reproduce figures and/or text from this article

View the Full Text HTML

J|A|C|S
COMMUNICATIONS

Published on Web 09/09/2005

Hierarchical Assembly of SnO_2 Nanorod Arrays on α-Fe_2O_3 Nanotubes: A Case of Interfacial Lattice Compatibility

Dong-Feng Zhang, Ling-Dong Sun,* Chun-Jiang Jia, Zheng-Guang Yan, Li-Ping You, and Chun-Hua Yan*

State Key Lab of Rare Earth Materials Chemistry and Applications, PKU-HKU Joint Lab in Rare Earth Materials and Bioinorganic Chemistry, and Electron Microscopy Laboratory, Peking University, Beijing 100871, China

Received July 16, 2005; E-mail: yan@pku.edu.cn

Composite nanomaterials are expected to have complex device functionalities due to their diverse properties, which can be tailored by fine-tuning the morphology, composition, and organization pattern of the primary nanobuilding blocks.[1] In recent years, progress has been made in the fabrication of nanocomposites with core−shell, coaxial nanocable, one- and two-dimensional (1D and 2D) heterojunction structures.[2] To explore the potential applications, however, architecturally assembling primary nanobuilding blocks into expected geometric forms is required. Despite the hierarchical complex structures achieved on ZnO/In_2O_3,[3] ZnO/TiO_2,[1b] SnO/SnO,[4] etc.,[5] a general scheme for the controlled organization and studies on the preferential crystallographic orientation of the secondary structure are lacking.

As important fundamental materials, SnO_2[6] and Fe_2O_3[7] have attracted great interest. It has been demonstrated that SnO_2-α-Fe_2O_3 binary oxide has better gas sensitivity than pure SnO_2 and α-Fe_2O_3.[8] In this paper, we presented a facile solution method to assemble SnO_2 nanorod arrays hierarchically on the surface of α-Fe_2O_3 nanotubes. Induced by the geometry of the α-Fe_2O_3 nanotubes, the heterostructures were of 6-fold symmetry. The crystallographic orientation at the interface was also studied.

α-Fe_2O_3 nanotubes were synthesized via a "coordination-assisted dissolution" process.[9] The nanotubes, with diameters of 100−110 nm, are bounded with six {110} planes (Figure S1); 0.01 g of α-Fe_2O_3 nanotubes was dispersed into a reverse micelle solution consisting of heptane (10.2 mL), hexanol (3.0 mL), sodium dodecyl sulfate (SDS, 1.44 g), and $Sn(OH)_6^{2-}$ ($V_{SnCl4,0.5mol/L}$:$V_{NaOH,5.0mol/L}$ = 1:2; 2.0 mL). After ultrasonication for 5 min, the mixture was transferred into a 25 mL Teflon-lined autoclave and heated to 220 °C for 6 h. When cooled to room temperature naturally, the resulting precipitates were collected by centrifugation and decanting and were washed several times with absolute ethanol and distilled water.

Figure 1a is a typical scanning electron microscopy (SEM) image of the product (a broad view is shown in Figure S2). It demonstrates that the products exhibit hierarchical structures, where the secondary nanorod arrays stand perpendicular to the side surfaces of the α-Fe_2O_3 nanotubes as multiple rows in a parallel manner. The 6-fold symmetry feature can be clearly observed from the image recorded from the cross-section of the nanocomposite (inset of Figure 1a). We proposed that the symmetry feature was determined by the hexagonal geometrical nature of the α-Fe_2O_3 nanotubes (inset of Figure S1a). Powder X-ray diffraction (XRD) patterns (Figure 1b) identified the composite as a mixture of α-Fe_2O_3 ($a = b = 4.36$ Å, $c = 13.75$ Å; JCPDS No. 33-0664) and tetragonal SnO_2 ($a = b =$ 4.75 Å, $c = 3.18$ Å; JCPDS No. 77-0450). To identify the local atomic composition of the heterostructures, nanoprobe X-ray energy dispersive spectrometry (EDS) was used. Figure 1d is the compositional profile line by scanning across an individual heterostructure

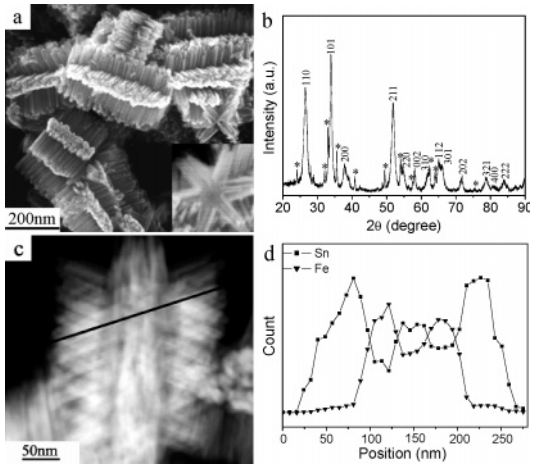

Figure 1. (a) SEM image; (b) XRD pattern of the composite; the asterisks indicate the peaks coming from α-Fe_2O_3 nanotubes, while the indexed ones are coming from SnO_2 nanocrystals. (c) Dark field image of an individual hierarchical structure. (d) Compositional profile line scanning along the dark line indicated in (c).

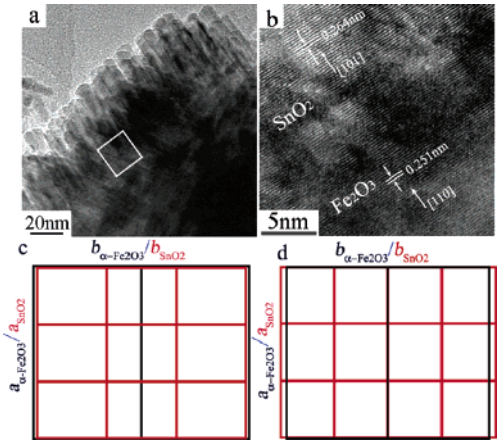

Figure 2. (a) A closer TEM observation from the interfacial region of an individual hierarchical structure. (b) HRTEM image recorded from the white frame in (a). (c, d) Schematics of the interfacial lattice mismatch between $\{110\}_{\alpha-Fe2O3}$ and [101], [001] growth of SnO_2, respectively.

along the black line in Figure 1c. It suggests that the secondary nanorods are pure SnO_2, which cover the α-Fe_2O_3 nanotubes.

The structure of the nanocomposite was further characterized by high-resolution TEM (HRTEM). Figure 2a displays the interface region of a typical hierarchical structure. Figure 2b is a HRTEM image recorded from the white frame of Figure 2a, with the electron beam irradiating perpendicular to the axis of the interface (also see Figure S3). The border between SnO_2 nanorods and α-Fe_2O_3 nanotubes is almost invisible, which suggests that composition

10.1021/ja054771k CCC: $30.25

fusion may occur at the interface. On the other hand, the lattice fringes parallel to the interface can be clearly observed. The spacing is 0.264 nm for the secondary nanorods and 0.251 nm for the inner nanotubes, corresponding to the (101) plane of tetragonal SnO_2 and the (110) plane of α-Fe_2O_3, respectively. It revealed that SnO_2 nanorods grew on the {110} planes of α-Fe_2O_3 with the interfacial orientation relationship as $(101)_{SnO2}/(110)_{\alpha-Fe2O3}$. The growth direction of the SnO_2 nanorods can be determined as [101]. Noteworthy, it differs from our previous report[10] that [001] is the preferential growth direction for SnO_2 nanorods obtained at a similar condition but without α-Fe_2O_3 nanotube directing.

To address how the α-Fe_2O_3 nanotubes had affected the growth direction of the SnO_2 nanorods, we compared the lattice mismatch of different interfacial orientations. For SnO_2 nanocrystals growing along [101], the interface is composed of $\{110\}_{\alpha-Fe2O3}$ and $\{101\}_{SnO2}$. The structure model of atomic arrangement (Figure S4a) shows that one period of $(001)_{\alpha-Fe2O3}$ and two of $(110)_{\alpha-Fe2O3}$ constitute a 2D unit cell in the $(110)_{\alpha-Fe2O3}$, with the lattice parameters of $a_{\alpha-Fe2O3} = 13.75$ Å and $b_{\alpha-Fe2O3} = 8.72$ Å, respectively. For $(101)_{SnO2}$, the 2D unit cell can be defined as $(010)_{SnO2}$ and the intercept of $(100)_{SnO2}$ in $(101)_{SnO2}$ (Figure S4b). From the geometry of the crystal structure, the corresponding lattice parameters can be determined as $a_{SnO2} = 4.75$ Å and $b_{SnO2} = 5.72$ Å, respectively. As shown in Figure 2c, the optimized lattice compatibility along the *a* direction is three a_{SnO2} matching to one $a_{\alpha-Fe2O3}$, with the lattice mismatch of $|(3a_{SnO2}-a_{\alpha-Fe2O3})/a_{\alpha-Fe2O3}| = 3.6\%$. Similarly, three b_{SnO2} match to two $b_{\alpha-Fe2O3}$ along the *b* direction, with the lattice mismatch of 1.6%. In the case of [001] growth of SnO_2, $(100)_{SnO2}$ and $(010)_{SnO2}$ are the low-indexed perpendicular planes. Since for tetragonal SnO_2, the *d* space of (100) is equal to that of (010) (4.75 Å), a square 2D unit cell can be found in $(001)_{SnO2}$. As shown in Figure 2d, although the lattice mismatch along the direction $a_{\alpha-Fe2O3}$ is the same as that of [101] growth SnO_2, that is, 3.6% with three a_{SnO2} matching to one $a_{\alpha-Fe2O3}$, while along the direction of $b_{\alpha-Fe2O3}$, the mismatch increases to as large as 8.9% with four b_{SnO2} matching to two $b_{\alpha-Fe2O3}$. Therefore, the decreased lattice mismatch should be responsible for the varied growth direction. In addition, the similar atomic arrangement in $\{110\}_{\alpha-Fe2O3}$ and $\{101\}_{SnO2}$ may further facilitate the formation of the composites (Figure S4c). As we know, (001) is the highest energy plane for rutile SnO_2, the deviated growth from it implied that the least interfacial lattice mismatch could lower the heteronucleation energy barrier and thus make it a key factor in determining the growth behavior of the secondary phase. Similar phenomena were also observed by Wang et al. in a VLS system.[11] The result may cast some light on the nucleation growth process in a heterogeneous system.

The length of the secondary nanorod can be modulated by controlling the reaction time (Figure S5). With the reaction time shorter than 0.5 h, only bare α-Fe_2O_3 nanotubes were observed. With the reaction prolonged to 1.5 h, a layer of nanoparticles with a thickness of few nanometers deposited on the surface of the α-Fe_2O_3 nanotubes. Extending the reaction to 6 h caused nanoparticles to grow into arrays of nanorods with a length of around 70 nm. The deposition of SnO_2 on the inner surface of α-Fe_2O_3 tubes took place simultaneously, and it reflected from the increased Sn signal inside the α-Fe_2O_3 tube domain in Figure 1d. Their lengths

Scheme 1. Illustration of the Composite Formation Process

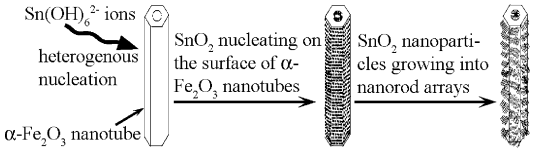

are restricted by the inner space of α-Fe_2O_3 tubes. The time-dependent experiments provided the information on the composite formation process vividly, which was depicted in Scheme 1. The whole process can be simplified into two stages: (1) SnO_2 nanoparticles nucleated on the surfaces of the α-Fe_2O_3 nanotubes. Driven by the decreased lattice mismatch, the SnO_2 nanoparticles took [101] as its preferential orientation. (2) With the dehydration of $Sn(OH)_6^{2-}$, SnO_2 nanoparticles anisotropically grew into nanorods to form hierarchical heterostructures with 6-fold symmetry.

In summary, SnO_2 nanorod arrays were hierarchically assembled onto the surface of α-Fe_2O_3 nanotubes by a facile solution method. Determined by the hexagonal geometry of the α-Fe_2O_3 nanotubes, the heterostructures were of 6-fold symmetry. HRTEM characterizations demonstrated that the lattice mismatch at the interface played an important role in determining the growth direction of the secondary nanorod arrays. The as-prepared SnO_2/α-Fe_2O_3 hierarchical assembly is a promising candidate with improved properties, such as gas sensitivity.

Acknowledgment. We thank NSFC (10374006, 20221101) and CPSF (2004036170) for the financial support.

Supporting Information Available: More SEM and HRTEM results. This material is available free of charge via the Internet at http://pubs.acs.org.

References

(1) (a) Sze, S. M. *Physics of Semiconductor Devices*; Wiley-Interscience: New York, 1981. (b) Yang, H. G.; Zeng, H. C. *J. Am. Chem. Soc.* **2005**, *127*, 270.
(2) (a) Gu, H. W.; Zheng, R. K.; Zhang, X. X.; Xu, B. *J. Am. Chem. Soc.* **2004**, *126*, 5664. (b) Lange, F. F. *Science* **1996**, *273*, 903. (c) Sorenson, T. A.; Morton, S. A.; Waddill, G. D.; Switzer, J. A. *J. Am. Chem. Soc.* **2002**, *124*, 7604. (d) Lincoln, J. L.; Mark, S. G.; Deli, W.; Lieber, C. M. *Nature* **2002**, *420*, 57. (e) Milliron, D. J.; Hughes, S. M.; Cui, Y.; Manna, L.; Li, J. B.; Wang, L. W.; Alivisatos, A. P. *Nature* **2004**, *430*, 190. (f) Yong, L.; Chim, W. K. *J. Am. Chem. Soc.* **2005**, *127*, 1487.
(3) Lao, J. Y.; Wen, J. G.; Ren, Z. F. *Nano Lett.* **2002**, *2*, 1287.
(4) Wang, Z. L.; Pan, Z. W. *Adv. Mater.* **2002**, *14*, 1029.
(5) (a) Dick, K. A.; Deppert, K.; Larsson, M. W.; Mårtensson, T.; Seifert, W.; Wallenberg, L. R.; Samuelson, L. *Nat. Mater.* **2004**, *3*, 380. (b) Lan, Z. H.; Liang, C. H.; Hsu, C. W.; Wu, C. T.; Lin, H. M.; Dhara, S.; Chen, K. H.; Chen, L. C.; Chen, C. C. *Adv. Funct. Mater.* **2004**, *14*, 233.
(6) (a) Law, M.; Kind, H.; Messer, B.; Kim, F.; Yang, P. *Angew. Chem., Int. Ed.* **2002**, *41*, 2405. (b) Cheng, B.; Russell, J. M.; Shi, W. S.; Zhang, L.; Samulski, E. T. *J. Am. Chem. Soc.* **2004**, *126*, 5972. (c) Dai, Z. R.; Pan, Z. W.; Wang, Z. L. *Adv. Funct. Mater.* **2003**, *13*, 9.
(7) (a) Park, J.; An, K.; Hwang, Y.; Park, J. G.; Noh, H. J.; Kim, J. Y.; Park, J. H.; Hwang, N. M.; Hyeon, T. *Nat. Mater.* **2004**, *3*, 891. (b) Rockenberger, J.; Scher, E. C.; Alivisatos, A. P. *J. Am. Chem. Soc.* **1999**, *121*, 11595.
(8) (a) Sorescu, M.; Diamandescu, L.; Tarabasanu-Mihailab, D.; Teodorescu, V. S.; Howard, B. H. *J. Phys. Chem. Solids* **2004**, *65*, 1021. (b) Reddy, C. V. G.; Cao, W.; Tan, O. K.; Zhu, W. *Sens. Actuators B* **2002**, *81*, 170.
(9) Jia, C. J.; Sun, L. D.; Yan, Z. G.; You, L. P.; Luo, F.; Han, X. D.; Pang, Y. C.; Zhang, Z.; Yan, C. H. *Angew. Chem., Int. Ed.* **2005**, *44*, 4328.
(10) Zhang, D. F.; Sun, L. D.; Yin, J. L.; Yan, C. H. *Adv. Mater.* **2003**, *15*, 1022.
(11) (a) Ding, Y.; Gao, P. X.; Wang, Z. L. *J. Am. Chem. Soc.* **2004**, *126*, 2066. (b) Wang, X. D.; Song, J. H.; Li, P.; Ryou, J. H.; Dupuis, R. D.; Summers, C. J.; Wang, Z. L. *J. Am. Chem. Soc.* **2005**, *127*, 7920.

JA054771K